Numerical Simulation of Thixoforming

A. Zavaliangos and A. Lawley

Processing of alloys and composites in the solid plus liquid range has advantages over casting, forging, and powder metallurgy techniques. The sensitivity of semisolid slurries to temperature variations and their history and rate dependent behavior, however, make process design and control difficult. Precise selection of die velocity, process temperature, and die design is necessary to produce satisfactory products. Therefore, a computational capability for the prediction of the rheological behavior of semisolid materials would be an invaluable tool in process design. This work presents preliminary results on numerical simulations of thixoforming operations. Constitutive models that are able to describe qualitatively the transient flow behavior of semisolid materials are implemented in a finite element program. Simple but realistic thixoforming operations are simulated. Weaknesses of currently available constitutive models and numerical techniques are identified and discussed.

Keywords
semisolid processing, thixoforming, modeling, finite element

1. Introduction

THIXOTROPY is defined as material behavior characterized by a reversible decrease of apparent viscosity due to the application of shear. Thixotropic behavior in semisolid alloy slurries was first observed by Flemings and his coworkers in the early 1970s (Ref 1, 2). In particular; it was found that if the alloy is agitated vigorously during slow cooling from the melt, the dendritic microstructure is destroyed and replaced by a microstructure consisting of equiaxed grains. These alloys behave thixotropically with apparent viscosities in the range of 10^{-2} to 10^{4} Pa · s. In general, metallic systems that possess a nondendritic microstructure can be formed to net shape in the semisolid state. In addition, this microstructure is maintained during solidification and partial remelting of the alloy. This property allows the decoupling of the forming step from the process that produces the equiaxed microstructure; i.e., there is no need to match the rate of production of the two processes. The process that produces the equiaxed microstructure can still benefit from the economy of scale, while at the same time small batch forming can be viable economically. Solidified billets can be transported, stored, and sectioned to smaller sizes. Reheated billets can then be formed in the semisolid range. In this case, the forming process is termed *thixoforming*.

Semisolid processing offers advantages over the competing processes of die casting and forging, as identified in Table 1. Interest in semisolid processing has increased recently because it became apparent that it provides an attractive route for fabricating particle or fiber reinforced composite materials (Ref 3). Although the feasibility of semisolid processing has been demonstrated, it has not been accepted widely. Two major difficulties are encountered in semisolid processing. The first difficulty is that the process that produces the nondendritic thixoworkable microstructure is slow and complicated. A number of routes capable of producing such a microstructure have been explored, including electromagnetic stirring and strain-induced melt activation (Ref 4). Spray casting is currently under evaluation as a source of material with a fine dendrite-free microstructure (Ref 5).

The second difficulty is that process control and optimization are essential. The sensitivity of the flow of semisolid materials to temperature and their strong history-dependent flow behavior necessitate careful selection of the process variables, such as ram velocity, die temperature, maximum load, and dwell time. Moreover, semisolid processing is often unsuccessful due to flow instabilities and problems associated with the combined flow and solidification process, e.g., turbulent flow, solid-liquid segregation, and premature freezing of the advancing slurry. Temperature gradients can cause nonuniform flow behavior, uneven flow, or premature flow. It is important to develop the necessary processing science base consisting of constitutive models describing the rheology of the semisolid state in terms of material and process parameters. In turn, the design and optimization of semisolid processes can benefit directly from modeling.

This paper presents a framework for the numerical simulation of thixoforming. We implemented constitutive models capable of describing important aspects of the flow and

Table 1 Comparison of forging, die casting, and semisolid processing

Process	Advantages	Disadvantages
Forging	Favorable microstructure; structural integrity	High loads; die wear; low shape complexity
Die casting	Complex shape capability; low force requirements	Turbulent flow; undesirable microstructure; residual porosity; entrapped gas; inferior mechanical properties
Semisolid processing	Complex shape capability; low force requirements; low porosity; acceptable microstructure; ease of handling; laminar flow	Requires careful control; liquid segregation possible

A. Zavaliangos and **A. Lawley,** Department of Materials Engineering, Drexel University, Philadelphia, PA 19104, USA.

This paper was originally presented at the Symposium "Particulate Materials in Rheological Applications," TMS 1993 Fall Meeting, Materials Week Program.

deformation of semisolid materials at medium and high volume fractions of solid. Simple first-order simulations of thixoforming operations were carried out successfully. This computational capability for the prediction of the rheological behavior of semisolid materials provides a firm basis for rational process design and control.

2. Mechanisms of Flow and Deformation of Semisolid Alloys

Three different types of material behavior in the semisolid range were identified.

At a *low volume fraction of solid*, g_s (~g_s < 0.2 to 0.3) interactions between the solid grains are small. The material behaves as a Newtonian viscous fluid. The viscosity can be predicted by the theories of Einstein (Ref 6) and Bachelor (Ref 7).

At a *medium volume fraction of a solid* (~0.2 to 0.3 < g_s < 0.6 to 0.7), increased resistance to flow and nonlinear viscous, history-dependent behavior are present due to strong interactions between the solid particles. Two types of interactions characterize the resistance to flow: (a) hydrodynamic interactions due to the relative motion of solid particles; (b) and agglomeration of the solid particles by a welding-type mechanism. Recent work on the behavior of semisolid materials is based on the assumption that the resistance to deformation of the sheared material reflects the level of agglomeration of the solid particles (Ref 8). The reduction of the apparent viscosity during continuous shearing was explained on the basis of a disagglomeration process (the disruption of the solid particle bonds). A simultaneous competing agglomeration mechanism is also active.

At a *high volume fraction of solid* (g_s > 0.6 to 0.7), a skeleton of solid particles is always formed, and the system can be considered as a porous solid saturated with liquid. In this case, macroscopic deformation is accommodated by the deformation of solid grains (although slipping of wetted solid grain boundaries can also offer a potential mechanism contributing to macroscopic strains). The relative motion of the liquid phase can lead to extensive liquid-solid segregation. The permeability of the porous skeleton depends on the square of a characteristic length scale (Ref 9), typically of the order of the center-to-center distance of the solid grains. Therefore fine scale microstructures will reduce solid-liquid segregation due to the associated low permeability.

The range between 0.5 and 0.75 volume fraction of solid appears to be optimum for thixoforming because it satisfies the following requirements: (a) The semisolid material must be under conditions that allow easy handling; i.e., a billet should be able to retain its shape for a period of time. Elimination of the need to handle liquid substances will simplify dramatically the equipment requirements. (b) The forming operation must be performed at the lowest possible temperature in order to minimize the porosity that usually appears during solidification. (c) The flow and deformation resistance should be low enough to permit filling of complex shaped dies without excessive force requirements.

The following section discusses two types of phenomenological models that can describe the behavior of semisolid materials at medium and high volume fractions of solid, respectively.

3. Modeling

3.1 *Medium Volume Fraction of Solid*

For low to medium volume fractions of solid, the basis of a tenable model is vested in the general description of the non-Newtonian history-dependent incompressible fluids, in which the Cauchy stress tensor, **T**, is given by (Ref 10):

$$\mathbf{T} = -p\,\mathbf{1} + \eta(\mathrm{II_D}, \mathrm{III_D})\mathbf{D} + B(\mathrm{II_D}, \mathrm{III_D})\mathbf{D}^2 \qquad \text{(Eq 1)}$$

where p is the pressure, **1** is the second-order identity tensor, and η and B are functions of the second and third invariants, $\mathrm{II_D}$ and $\mathrm{III_D}$, of the stretching rate tensor **D**. This general form can be simplified if it is assumed that normal stress effects are negligible, i.e., $B = 0$. Also the dependence of η on $\mathrm{III_D}$ is usually ignored. In order to include structure effects, the parameter η should be a function of the internal variables λ_i and the temperature θ. Equation 1 can be written as:

$$\mathbf{T} = \eta(\mathrm{II_D}, \theta, \lambda_i)\,\mathbf{D} - p\,\mathbf{1} \qquad \text{(Eq 2)}$$

The model can then be complemented by an evolution equation for the internal variables λ_i:

$$\dot{\lambda}_i = \mathbf{g}_i\,(\mathrm{II_D}, \theta, \lambda_j) \qquad \text{(Eq 3)}$$

Heating due to shear is introduced by a term $\mathbf{T} \cdot \mathbf{D}$ in the energy balance, and the latent heat should be taken into account for nonisothermal calculations.

Martin, Kumar, and Brown (Ref 11) have introduced an internal variable framework to represent the rheological behavior of semisolid alloys and derived, from first principles, an expression for the apparent viscosity, which reflects the contributions from the hydrodynamics of the flow and the disruption of particle bonds:

$$\eta = \eta_1 + \eta_2 \qquad \text{(Eq 4)}$$

$$\eta_1 = A(\lambda)\frac{(c/c_{max})^{1/3}}{1 - (c/c_{max})^{1/3}}\eta_{liquid} \qquad \text{(Eq 5)}$$

$$\eta_2 = (n+1)C_0 \exp\left(\frac{nQ}{R\theta}\right) g_s\,\lambda\,\eta_{liquid}^{n+1}\,\dot{\gamma}^{n-1} \qquad \text{(Eq 6)}$$

where $A(\lambda)$ is a function of structure and reflects the effect of structure on the hydrodynamic part of viscosity; $c(\lambda) = g_s(1 + \alpha\lambda)$ is an effective volume fraction of solid; α is a constant; g_s is the volume fraction of solid; $c_{max} = 0.64$; $\tau/\tau_0 = \exp(Q/(R\theta))\,(\dot{\gamma}/\dot{\gamma}_0)^n$ is the temperature dependent power law

Table 2 Material properties for Sn-15wt % Pb at 460 K

n	4.	R_s	$9 \times 10^{-11}\, g_s^{4.702}$
Q	74.5 kJ	c	$1 + 0.1\,\lambda$
η	0.0025 Pa · s	c_{max}	0.64
C_0	1.97×10^{-28}	$A(\lambda)$	$24\lambda + 16$
H	$1.46\, g_s^{5.812}$	...	...

Table 3 Material properties representative of aluminum alloys in the semisolid range

A	8×10^{11}/s
Q	167. kJ
η	0.001 Pa · s
n	5.
s	32 MPa
K/η_{liquid}	$5 \times 10^{-8}\, g_L^2 m^2/(Pa \cdot s)$

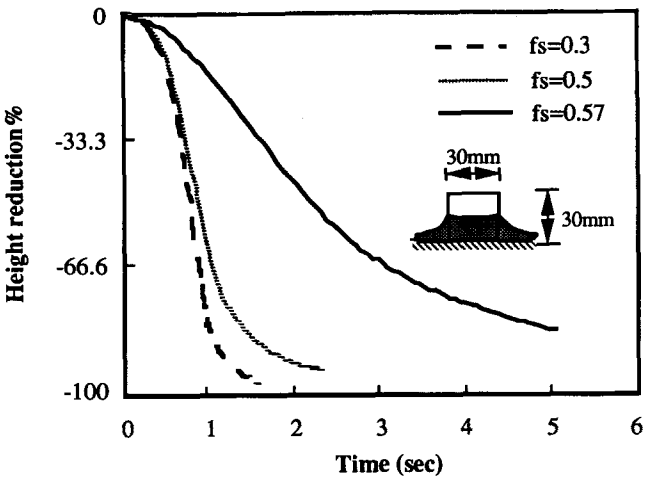

Fig.1 Prediction of flow of a free standing Sn-15%Pb billet under its own weight.

stress-strain rate governing the plasticity of the solid phase; n is the power law exponent; R is the universal gas constant; Q is an activation energy; and λ is the internal variable (a pure number) that represents the level of agglomeration in the slurry and takes values between 0 (no agglomeration) and 1 (full agglomeration). An evolution equation of the structure was also proposed by Martin, Kumar, and Brown (Ref 11):

$$\dot{\lambda} = H(g_s)(1 - \lambda) - R_s(g_s)\lambda\dot{\gamma}^n \qquad \text{(Eq 7)}$$

where λ represents the state of agglomeration in the semisolid mixture. The two terms represent the agglomeration and disagglomeration rates, respectively.

3.2 *High Volume Fraction of Solid*

The volume fraction of solid that corresponds to the close-packed configuration is the upper limit of validity of the model presented in the previous section. At high volume fractions of solid, a porous skeleton forms and provides resistance to deformation. The application of external pressure results in (a) a tendency for densification of the porous skeleton and (b) the development of pressure in the liquid. The latter case causes the liquid phase to flow relative to the solid phase toward regions of low pressure (e.g., free surfaces). These combined deformation and flow phenomena can be described mathematically by a theoretical framework suitable for deformable fully saturated porous media. This idea was recognized early, and one-dimensional version of such models were presented (Ref 12, 13). This paper presents an improved three-dimensional version of the model intended for modeling the flow and deformation of semisolid materials with a high volume fraction of solid. It consists of three parts: porous viscoplasticity model, fluid flow in a porous medium, and continuity equations.

3.2.1 Porous Viscoplasticity Model

The ideal of effective stress $\mathbf{T}^* = \mathbf{T} - p_{liquid}\,\mathbf{1}$ ($\mathbf{T}$ = macroscopic Cauchy stress, p_{liquid} = pressure in the liquid phase) can be employed together with a porous viscoplasticity model in order to describe the macroscopic deformation of the material.

A proper description of the highly rate-dependent behavior of the solid skeleton must be included in the model. Earlier efforts (Ref 12, 13, 14) employed extensions of rate-independent porous plasticity models (Ref 15, 16). Recently, Zavaliangos and Anand (Ref 17) presented a consistent temperature and rate-dependent framework capable of describing correctly rate effects in porous plasticity. Briefly, the flow rule is given by:

$$\mathbf{D}^p = \frac{\partial \Phi}{\partial \mathbf{T}} \qquad \text{(Eq 8)}$$

where $\mathbf{D}^p$ is the plastic stretching rate, $\Phi = \hat{\Phi}(\Sigma_e, \Sigma_h, s, g_L, \theta)$ is a viscoplastic potential (i.e., a generalization of the yield function for rate-dependent materials), Σ_h is the pressure, Σ_e is the equivalent stress, s is a measure of the deformation resistance of the solid (flow stress), θ is the temperature, and g_L is the volume fraction of liquid (or the porosity equivalent). In the fully dense solid phase, the flow potential and the equation for the plastic stretching have the classical power law form:

$$\Phi_d = \frac{\dot{\varepsilon}_0 s}{n+1} \exp\left(-\frac{Q}{R\theta}\right)\left(\frac{\Sigma_e}{s}\right)^{n+1} \qquad \text{(Eq 9)}$$

For porous materials, the existence of a potential is postulated:

$$\Phi = F(X, g_L, n)\,\Phi_d \qquad \text{(Eq 10)}$$

The function F accounts for the presence of porosity, and $X = \Sigma_h/\Sigma_e$ is the stress triaxiality. A recently proposed form for the function F (Ref 17) is:

$$F = A_1 + (A_2 X + A_3)^{(n+1)/2} \qquad \text{(Eq 11)}$$

where A_i refers to functions of porosity and the power exponent n. Here we adopt the forms for A_1, A_2, and A_3 proposed by

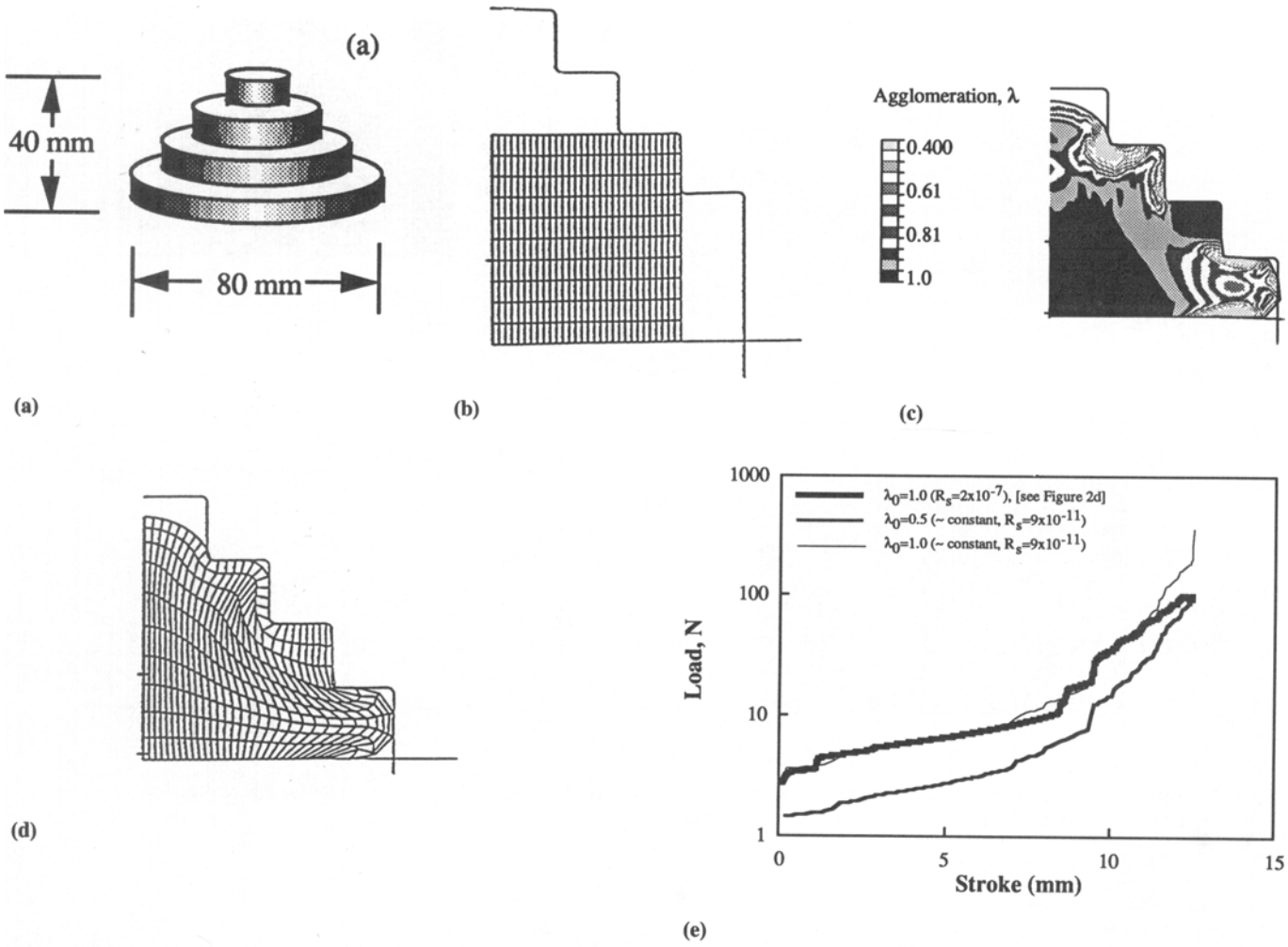

Fig. 2 Die filling with a semisolid alloy ($g_S = 0.55$): (a) specimen geometry, (b) undeformed finite element mesh, (c) deformed finite element mesh, (d) state of agglomeration near complete filling (simulation with $\lambda_0 = 1.$ and $R_S = 2 \times 10^{-7}$, and (e) load vs. stroke.

Zavaliangos and Anand (Ref 17). Modification of these forms is necessary to account for the effect of the shape and interconnectivity of the pores as well as for the evolution of the characteristics of porosity with very large strains.

3.2.2 Fluid Flow in a Porous Medium

The D'Arcy equation can be employed for describing liquid flow with respect to the solid phase:

$$\mathbf{v} = -\frac{K}{\eta_{\text{liquid}}(1 - g_L)}\left(\frac{\partial p_{\text{liquid}}}{\partial \mathbf{x}} - \rho_{\text{liquid}} g \hat{\mathbf{z}}\right) \qquad \text{(Eq 12)}$$

where $\mathbf{v}$ is the velocity of the liquid relative to the solid, η_{liquid} is the viscosity of the liquid phase, ρ_{liquid} is the liquid density, g is the acceleration of gravity, and K is the permeability of the porous medium. A simple model for permeability is given by:

$$K = \frac{g_L^2}{24\pi n \tau^3} \qquad \text{(Eq 13)}$$

where τ is the tortuosity factor, which takes into account the fact that the channels in which the liquid phase flows are neither straight nor symmetrical; n is the number of channels per unit area, which is proportional to the inverse of the square of the interchannel distance, e.g., proportional to the size of the solid grains for equiaxed microstructures, or the dendrite spacing for a dendritic microstructure. An important consequence of this definition is that smaller grain microstructures reduce the tendency for solid-liquid separation.

3.2.3 Continuity Equations

In order to couple properly the deformation of the porous skeleton and the flow of the liquid phase, continuity equations for both phases must be written.

For the liquid phase:

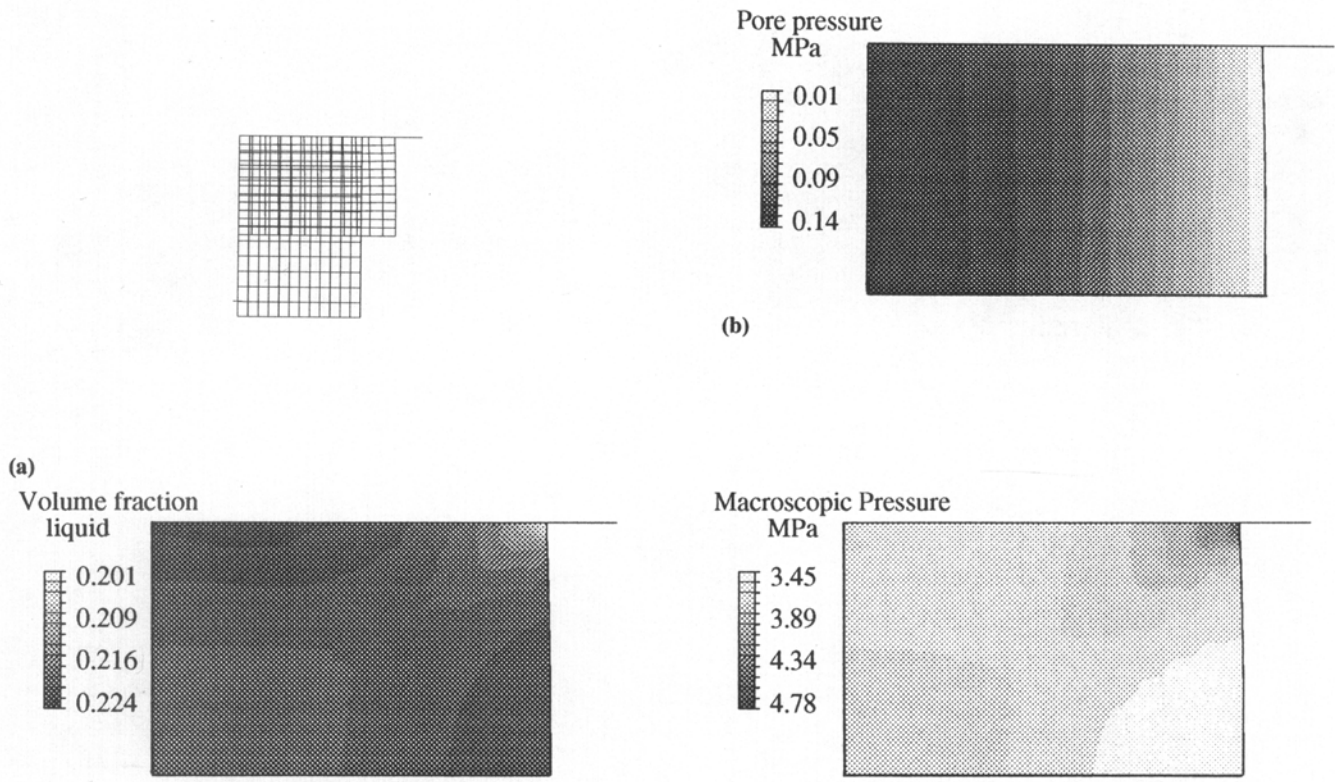

Fig. 3 Simple compression of a semisolid billet $g_s = 0.7$, low friction): (a) finite element mesh, (b) contours of pore pressure, (c) contours of volume fraction of liquid, and (d) contours of macroscopic pressure.

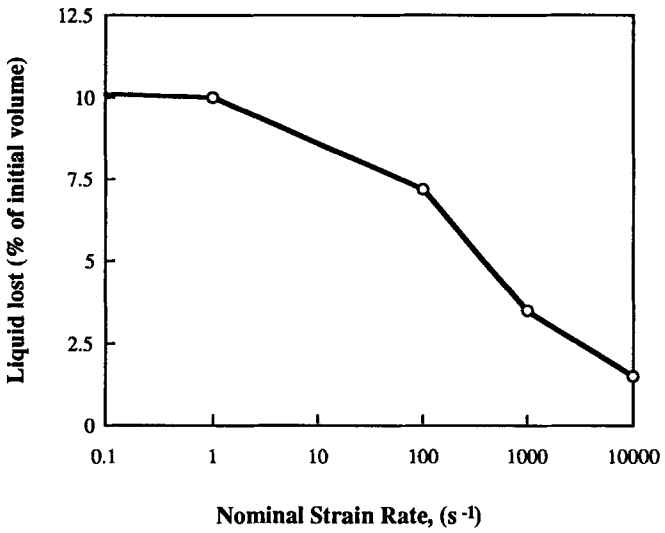

Fig. 4 Effect of strain rate on the loss of liquid phase during simple compression of a semisolid billet.

$$\frac{\partial(\rho_L g_L)}{\partial t} = -\nabla \cdot [\rho_L g_L (\mathbf{U}_s + \mathbf{v}_L)] \qquad \text{(Eq 14)}$$

For the solid phase:

$$\frac{\partial(\rho_s g_s)}{\partial t} = -\nabla \cdot (\rho_s g_s \mathbf{U}_s) \qquad \text{(Eq 15)}$$

Solidification requires an additional term in the continuity equations. Additional terms to account for the change is density due to the shift of composition are also necessary.

4. Simulation Results

The predictive capacities of the models presented are demonstrated in three examples: (a) flow of a free standing, semisolid billet with medium volume fraction of solid under its own weight; (b) thixoforming of a semisolid billet with $g_s = 0.55$; and (c) compression of a semisolid billet with $g_s = 0.70$. The models presented were implemented in ABAQUS, which is a commercial Lagrangian, displacement based finite element program. One restriction associated with this selection is that simulation with the nonlinear fluid model are restricted to "slow" (nonturbulent) types of flow. It is fortunate though that in the volume fraction of interest for thixoforming, flow is typically nonturbulent due to the relatively high viscosity of the slurry. It may be argued that Eulerian or perhaps Arbitrary Lagrangian Eulerian formulations are more suitable. Our selection was based mainly on the local availability of software. The numerical simulation of thixoforming is associated with some

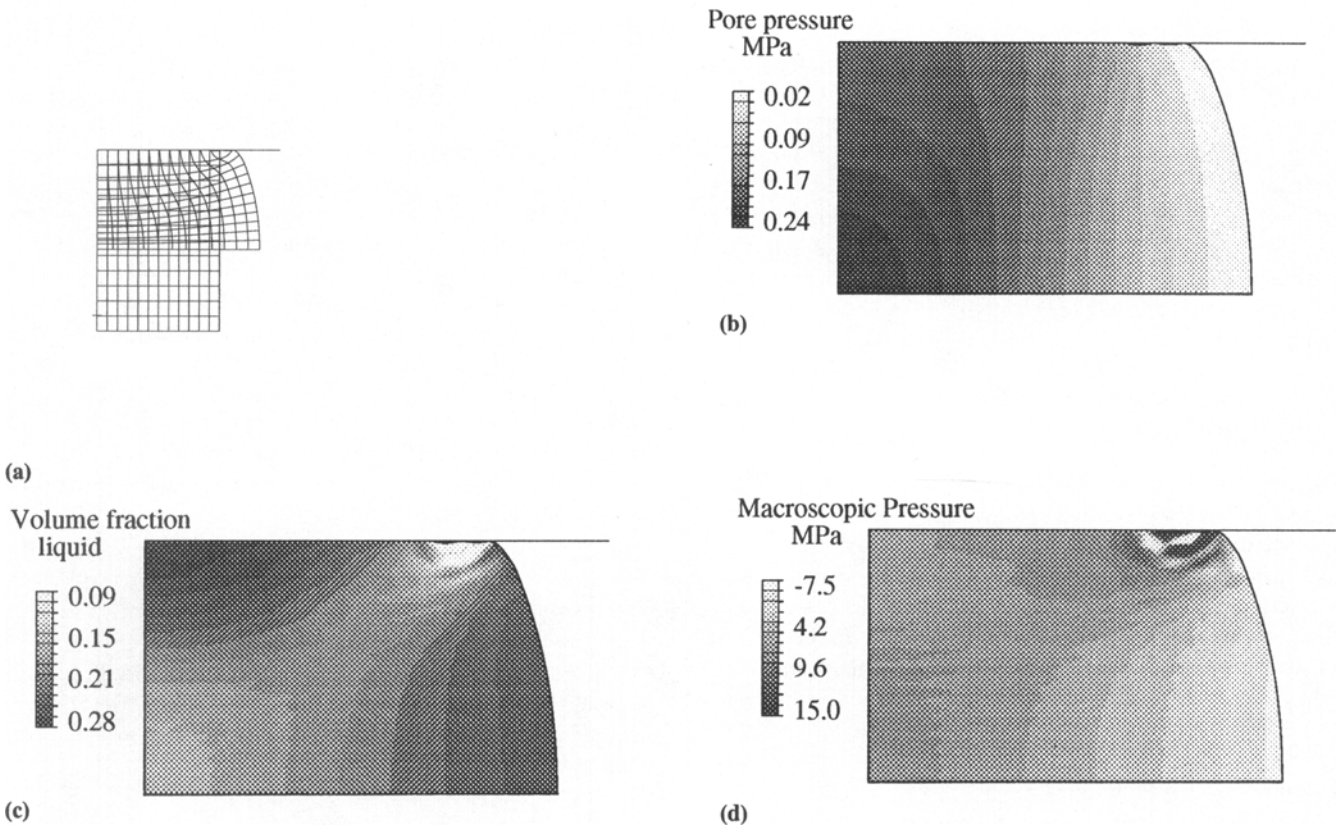

Fig. 5 Simple compression of a semisolid billet ($g_s = 0.7$, high friction): (a) finite element mesh, (b) contours of pore pressure, (c) contours of volume fraction of liquid, and (d) contours of macroscopic pressure.

of the most difficult numerical issues, such as moving surfaces, contact, friction, very large strains, significant material nonlinearities, and history dependence. Different approaches can accommodate some of the above, but there is no commercial software that can address them simultaneously in a satisfactory way.

4.1 *Free Standing Billet*

The ability of a semisolid billet to withstand its own weight is important because it allows for convenient handling and transportation. The isothermal simulation presented here is based on the model of Martin, Kumar, and Brown (Ref 11), with the solid particles fully agglomerated ($\lambda = 1$) and inertia included. Material properties employed in this calculation correspond to those of a Sn-15wt%Pb alloy (see Table 2) (Ref 1). The results of this isothermal simulation demonstrate that for volume fractions of $g_s < 0.5$, the resistance to flow is minimal, mainly due to inertia effects; see Fig. 1. The billet acquires a significant resistance to flow only when the volume fraction of solid is close to the percolation limit, where a solid skeleton forms throughout the volume of the specimen.

Experimental observations indicate that at volume fractions $0.5 < g_s < 0.6$, the resistance to flow of the semisolid material is characterized by spikes, which correspond to particle bridging between stationary and nonstationary boundaries. It is clear that percolation-type arguments can justify such behavior, which depends on the ratio of internal over external characteristic lengths, e.g., the ratio of grain diameter to specimen dimensions. The transition from fluid-like behavior to saturated porous material behavior and its mathematical description is an open issue.

4.2 *Simple Thixoforming Operation*

The key advantage of thixoforming is the ability to achieve die filling at temperatures much lower than the liquidus. In this example, we demonstrate the ability to simulate die filling operations. The forming of a component shown in Fig. 2(a) was simulated. This geometry was selected (Ref 18) to demonstrate the ability of semisolid materials to fill complex cavities with reasonable force requirements. It is very difficult to produce such geometry by forging.

The selected material parameters correspond to those of Sn-15wt%Pb at 460 K (volume fraction of solid $g_s \cong 0.55$) and are shown in Table 2 (Re 8). The initial value of the internal variable λ was taken to be 1. Figure 2(b) shows the undeformed mesh geometry. Figure 2(c) shows the deformed mesh just before complete die filling at a force of about 1 kN and a die velocity of 1.5 m/s. The initial structure plays a critical role. Figure 2(e) shows computed force and stroke curves for two different values of the initial level of agglomeration, $\lambda = 0.5$ and $\lambda = 1$. For the material parameters of Sn-15wt%Pb, there is negligible disagglomeration during the forming step. Knowl-

edge and control of the initial state is essential for the prediction and optimization of the die filling process. To demonstrate the effects of disagglomeration, we ran a simulation with $\lambda = 1$ and a new value for the parameter $R_s = 2 \times 10^{-7}$ (Eq 7), which controls the rate of disagglomeration. Such a high value for R_s accelerates disagglomeration. Contours of the internal variable λ obtained from this simulation are shown in Fig. 2(d). Disagglomeration occurs where the material is heavily deformed, resulting in reduced flow resistance and lower force requirements; see Fig. 2(e).

4.3 *Compression of a Semisolid Billet—Strain Rate and Frictional Effects*

Compression experiments on semisolid alloys were performed by Flemings et al. (Ref 12, 14) in order to characterize the behavior of semisolid materials at high volume fractions of solid. Among the important results of these experiments are (a) the increased liquid-solid segregation with decreased strain rate, and (b) significant effects due to friction. In this simulation, we reproduce these observed experimental phenomena and confirm the validity of the theoretical modeling approach. Simulations described in this section were performed using the material parameters listed in Table 3; these are representative of aluminum alloys.

We have simulated numerically simple compression tests under different frictional conditions over a range of imposed nominal strain rates. The geometry of the problem is shown in Fig. 3(a). Only a quarter of the specimen is modeled due to symmetry. Figure 3(b) shows the pore pressure gradient, which develops along the radial direction in the case of low friction ($\mu = 0.01$) at a strain rate of 100/s. After a strain of 0.6, a significant amount of liquid was expelled (~0.1 vol%). The variation of the volume fraction of liquid is minimal; see Fig. 3(c).

In order to demonstrate the effect of strain rate on the retention of liquid, we repeated the simulations for a range of strain rates. The variation of expelled liquid with the imposed strain rate is shown in Fig. 4. As expected, the simulation predicts that at higher strain rates, less liquid is lost. This is a very important observation for thixoforming and must be exploited in the selection of process parameters.

Simulations with sticking friction were performed. Figure 5 shows the variation of the volume fraction of liquid in a semisolid billet compressed to $\varepsilon = 0.6$ at $\dot{\varepsilon} = 100/s$. A significant variation of g_L is observed over the volume of the specimen. This situation is undesirable because it leads to a variation of the local alloy composition and implies unwanted variability of the local properties.

Friction between a semisolid alloy and a rigid die is expected to be governed by the state of the surface of the billet (e.g., the presence or absence of oxidation film), the local properties of the semisolid material (e.g., volume fraction of solid, and permeability), and the stress state (e.g., normal stress on the surface, and pressure in the liquid). Clearly the usefulness of a Coulomb type model is limited. More work is needed to understand and develop an accurate description of the friction on semisolid materials.

5. Conclusions

We presented a constitutive framework capable of describing several important aspects of the flow and deformation of semisolid materials. Specific models were implemented in a finite element code, and simulations of thixoforming operations were carried out. Observed experimental trends, such as the effect of strain rate on liquid retention, were verified by numerical simulations.

It is important to stress the preliminary nature of these results. Significant effort must be focused on understanding the underlying physical mechanisms of deformation in the case of high volume fractions of solid. Several other issues remain open: (a) interpolation in the transition between the medium and high volume fraction models, (b) modeling of friction, (c) extension to nonisothermal calculations, and (d) extension to composite semisolid slurries.

Acknowledgments

Support for this work was provided by the Civil and Mechanical Systems Division of the National Science Foundation (grants No. MSS-9007392 and MSS-9313254). The finite element code ABAQUS was available under an academic license to Drexel University from HKS, Inc., Pawtucket, RI.

References

1. D.B. Spencer, R. Mehrabian, and M.C. Flemings, Rheological Behavior of Sn-15%Pb in the Crystallization Range, *Metall. Trans.*, Vol 3, 1972, p 1925-1932
2. M.C. Flemings, Behavior of Metal Alloys in the Semisolid State, *Metall. Trans. A*, Vol 22, 1991, p 957-981
3. F.A. Girot, L. Albingre, J.M. Quenisset, and R. Naslain, Rheocasting Al Matrix Composites, *J. Met.*, Nov 1987, p 18-21
4. M.P. Keney, J.A. Courtois, R.D. Evans, G.M. Farrier, C.P. Kyonka, A.A. Koch, and K.P. Young, *Metals Handbook*, 9th ed., Vol 15, ASM International, 1988, p 327-338
5. P.Kapranos and D.H. Kirkwood, Semisolid Processing of Alloys, *Met. Mater.*, Vol 15 (No. 1), Jan 1989, p 16-19
6. A. Einstein, *Ann. Phys.*, Vol 19, 1906, p 289
7. G.K. Bachelor, The Effect of Brownian Motion the Bulk Stress in a Suspension of Spherical Particles, *J. Fluid Mech.*, Vol 83, 1977, p 97
8. P. Kumar, C. Martin, and S.B. Brown, Shear Rate Thickening Behavior of Semisolid Slurries, *Metall. Trans. A*, Vol 24, 1993, p 1107-1116
9. T.S. Piwonka and M.C. Flemings, Pore Formation in Solidification, *Metall. Trans. AIME*, Vol 236, 1966, p 1157
10. R.S. Rivlin, *Proc. R. Soc. A*, Vol 193, 1948, p 260-281
11. C. Martin, P. Kumar, and S.B. Brown, Shear Rate Thickening Flow Behavior of Semisolid Slurries, *Metall. Trans. A*, Vol 24, 1993, p 1107-1116
12. P.O. Charreyron and M.C. Flemings, Rheology of Semisolid Dendritic Sn-Pb Alloys at Low Strain Rates: Application to Forming Process, *Int. J. Mech. Sci.*, Vol 27, 1985, p 781-791
13. L.A. Lalli, A Model for Deformation and Segregation of Solid Liquid Mixtures, *Metall. Trans. A*, Vol 16, 1985, p 1393-1403
14. M. Suery and M.C. Flemings, Effect of Strain Rate on Deformation Behavior of Semi-Solid Dendritic Alloy, *Metall. Trans. A*, Vol 13, 1982, p 18091819

15. S. Shima and M. Oyane, Plasticity Theory for Ductile Metals, *Int. J. Mech. Sci.*, Vol 18, 1976, p 285-291

16. H.A. Kuhn and C.L. Downey, Deformation Characteristics and Plasticity Theory of Sintered Powder Materials, *Int. J. Powder Metall.*, Vol 7, 1971, p 15-25

17. A. Zavaliangos and L. Anand, Thermo-Elastic-Viscoplasticity of Porous Isotropic Metals, *J. Mech. Phys. Solids*, Vol 41 (No. 6), 1993, p 1087-1118

18. Osprey Metals Ltd., European Patent No. 0200349, 1985; U.S. Patent No. 4804034, 1987